Evaluating spatio-temporal soil erosion dynamics in the Winam Gulf catchment, Kenya for enhanced decision making in the land-lake interface

Olivier S. Humphrey[1], Odipo Osano[2], Christopher M. Aura[3], Andrew L. Marriott[1], Sophia M. Dowell[1,4], William H. Blake[4] and Michael J. Watts[1]

[1]Inorganic Geochemistry, British Geological Survey, Nottingham, NG12 5GG, UK

[2]School of Environmental Sciences, University of Eldoret, Eldoret, Kenya

[3]Kenya Marine and Fisheries Research Institute (KMFRI), P.O. Box 1881, Kisumu, Kenya

[4]School of Geography, Earth and Environmental Sciences, Plymouth University, UK

[*]Corresponding author: O. S. Humphrey; email: olih@bgs.ac.uk, telephone number: 0115 936 3336

Highlights

- Dynamic soil erosion rates were estimated using monthly rainfall and NDVI datasets
- The greatest risk of soil erosion occurs between February and April
- Reduced vegetation cover leads to greater soil erosion susceptibility
- Soil erosion hotspots were identified and should be the focus of future investigations
- Gross soil loss through erosion amounts to 10.71 Mt $year^{-1}$

Abstract

Soil erosion accelerated by poor agricultural practices, land degradation, deprived infrastructure development and other anthropogenic activities has important implications for nutrient cycling, land and lake productivity, loss of livelihoods and ecosystem services, as well as socioeconomic disruption. Enhanced knowledge of dynamic factors influencing soil erosion is critical for policymakers engaged in land use decision-making. This study presents the first spatio-temporal assessment of soil erosion risk modelling in the Winam Gulf, Kenya using the Revised Universal Soil Loss Equation (RUSLE) within a geospatial framework at a monthly resolution between January 2017 and June 2020. Dynamic rainfall erosivity and land cover management factors were derived from existing datasets to determine their effect on average monthly soil loss by water erosion. By assessing soil erosion rates with enhanced temporal resolution, it is possible to provide greater knowledge regarding months that are particularly susceptible to soil erosion and can better inform future strategies for targeted mitigation measures. Whilst the pseudo monthly average soil loss was calculated (0.80 t ha^{-1} $month^{-1}$), the application of this value would lead to misrepresentation of monthly soil loss throughout the year. Our results indicate that the highest erosion rates occur between February and April (average 0.95 t ha^{-1} $month^{-1}$). In contrast, between May and August, there is a significantly reduced risk (average 0.72 t ha^{-1} $month^{-1}$) due to the low rainfall erosivity and increased vegetation cover as a result of the long rainy season. The mean annual gross soil loss by water erosion in the Winam Gulf catchment amounts to 10.71 Mt $year^{-1}$, with a mean soil loss rate of 9.63 t ha^{-1} $year^{-1}$. These findings highlight the need to consider dynamic factors within the RUSLE model and can prove vital for identifying areas of high erosion risk for future targeted investigation and conservation action.

Graphical Abstract

Keywords: RUSLE, GIS, Remote Sensing, Soil Erosion, Winam Gulf, Kenya

1. Introduction

Soil erosion is one of the greatest global threats to water and food security (Amundson et al., 2015; Borrelli et al., 2017; Igwe et al., 2017). Within East Africa's interlacustrine countries of Burundi, Kenya, Rwanda, Tanzania and Uganda soil erosion is the main cause of land degradation to agricultural and pastoral landscapes (Wynants et al., 2019). Land degradation caused by soil erosion leads to the loss of nutrient rich surface soils, decreased soil fertility and increased runoff with severe consequences for food, water and livelihood security (Blaikie and Brookfield, 2015; Obalum et al., 2012; Oldeman, 1992; Pimentel, 2006; Vrieling, 2006). Sub-Saharan Africa has experienced rapid and extensive land-use change; between 1975 and 2000 16% of forested areas were lost, whilst agricultural land expanded 55% (Brink and Eva, 2009). As natural vegetation cover is displaced, rainfall infiltration capacity decreases, which results in increased surface runoff contributing to high, nutrient rich sediment loads in rivers (Van Oost et al., 2000; Zuazo and Pleguezuelo, 2009). Moreover, the increased frequency of extreme weather events occurring due to climate change will significantly influence the intensity of precipitation, increasing the energy available in rainfall for eroding soils (Maeda et al., 2010). Yang et al. (2003) predicted that global average soil erosion would increase approximately 9% by 2090 due to climate change. Whilst soil erosion is a natural process, accelerated rates of soil loss, compounded by poor land management practices and changes to vegetation cover and rainfall intensity, represent serious environmental issues. Increased rates of soil erosion are directly associated with nutrient loss, negatively influencing agricultural productivity and causing eutrophication of aquatic systems, threatening food security (Bakker et al., 2007; Istvánovics, 2010; Maeda et al., 2010).

Estimating the risk of soil erosion is critical to enable policymakers to implement land-use decisions aimed at mitigating the loss of soil substrate. Substantial efforts have been made to develop soil erosion models as useful tools for obtaining a baseline to which alternative land use management strategies can be applied (Ganasri and Ramesh, 2016; Nearing et al., 2005). Multiple soil erosion models exist with varying degrees of complexity. The most widely applied empirical model for investigating soil erosion is the Revised Universal Soil Loss Equation (RUSLE). The model is formulated as the compound product of multiple single layers; rainfall erosivity (R factor), soil erodibility (K factor), topography (LS factor), cover management (C factor), and support practices (P factor), which creates a single soil erosion risk map. This model has been widely applied to assess the risk of soil erosion and estimate soil loss around the globe (Chen et al., 2011; Kouli et al., 2009; Lu et al., 2004; Panagos et al., 2014b; Prasannakumar et al., 2012) and while there are caveats in terms of rate quantification, it remains a valuable tool for evaluating spatial variability and areas of relatively high risk. The model, calculated and integrated using remote sensing data and geographical information systems (GIS), enables soil erosion risk mapping to become feasible with sufficient accuracy and precision in large basin-scale and regional studies (Magesh and Chandrasekar, 2016). Conventional methods used to assess soil erosion risk are expensive, time consuming and have poor spatial resolution. The RUSLE model approach can predict erosive potential with detailed spatial assessment and characterisation within large areas. However, the majority of RUSLE model applications are somewhat limited by presenting a singular erosion map of time averaged data. Whilst soil erodibility and topographic factor maps are relatively static (excluding large scale geogenic or anthropogenic induced land alterations), high intra-annual variability is expected for rainfall and cover management factors due to the natural patterns of precipitation and vegetation growth (Panagos et al., 2012; Schmidt et al., 2019; Wang et al., 2001).

The importance of capturing spatial variability within a soil erosion model is not a revolutionary concept. Wischmeier and Smith (1965) advocated that soil erosion risk modelling should be assessed with a monthly temporal resolution. However, due to the lack of availability of high temporal resolution spatial datasets, the application of this method is limited. Recent studies have integrated dynamic variables into soil risk erosion modelling, such as R factors (Angulo-Martínez and Beguería, 2009; Ballabio et al., 2017; Ma et al., 2014; Nunes et al., 2016) and C factors (Alexandridis et al., 2015; Schmidt et al., 2018; Yang, 2014) to assess intra-seasonal and annual changes to soil erosion. However, the application of combining dynamic R and C factors for assessing soil over multiple years has not previously been assessed. Quantifying soil loss on a dynamic time scale will develop a wider understanding, and allow for the implementation of targeted protection measures for susceptible hotspots during particularly high-risk seasons (Schmidt et al., 2019; Troxler et al., 2004). In this study, we aim to create a dynamic soil erosion map for the Winam Gulf catchment of Lake Victoria in Kenya, with the following objectives: (1) Use of monthly R and C factors to delineate inter- and intra-annual spatio-temporal patterns of soil erosion; and (2) identify soil erosion hotspots within the catchment to inform ground-truthing surveys and mitigation strategies.

2. Materials and Methods

2.1 Study Site

The study area was the Winam Gulf catchment (0°38'S-0°10'N, 34°8'E-35°33'E), with an approximate area of 11,000 km^2, located in western Kenya (Figure 1). The Winam Gulf catchment comprises four sub-basins; (i) the Northern Shore, which is relatively flat; (ii) the Nyando, which contains the Nandi Hills; (iii) the Sondu, with low plains near the lakeshore and a mountainous region eastward, and; (iv) the Southern Shore, which is dominated by extinct volcanic masses (Mt Homa, Gembe Hills and Gwassi Hills). The dominant soil groups in the region are acrisols, cambisols, and vertisols (IUSS Working Group, 2014). The study area experiences an equatorial climate with dipole rainy seasons which occur in March to May (long rainy season) and October to November (short rainy season). Therefore, there is significant interannual variation in the volume and duration of rainfall in the region with the annual average precipitation between 600 and >2000 mm; the annual average temperature varies between 17.4-29.9 °C (Calamari et al., 1995; Fusilli et al., 2013; Okungu et al., 2005). Historic land use within the catchment area was predominantly natural vegetation (61.8 %), followed by agricultural land (32.5 %) and infrastructure/miscellaneous land use (5.7%) (Calamari et al. 1995).

Figure 1 Elevation map of the Winam Gulf catchment, Kenya and its major sub-basins: (A) Northern Shore, (B) Nyando, (C) Sondu, and (D) Southern Shore. Roman numerals represent specific landforms within the Winam Gulf catchment: (i) Nandi Hills, (ii) Kisumu Basin, (iii) Mt Homa, (iv) Gembe Hills, and (v) Gwasshi Hills

2.2 Erosion risk assessment using RUSLE

Assessment of the soil erosion risk within the Winam Gulf catchment was performed in ArcGIS (version 10.7) using the Revised Universal Soil Loss Equation (RUSLE) (Renard et al., 1997; Wischmeier and Smith, 1978), which calculated soil loss rates by sheet and rill erosion using the following Eq. 1:

$$A = R \times K \times LS \times C \times P \quad (1)$$

where A is the annual average soil loss (t ha^{-1} yr^{-1}); R is the rainfall erosivity factor (MJ mm ha^{-1} h^{-1} yr^{-1}); K is the soil erodibility factor (t ha h ha^{-1} MJ^{-1} mm^{-1}); LS is the slope length and steepness factor (dimensionless); C is the cover management factor (dimensionless, ranging between 0 and 1); and P is the support practice factor (dimensionless, ranging between 0 and 1). The equation can be modified to a monthly soil loss equation by including a monthly temporal resolution for the dynamic R (MJ mm ha^{-1} h^{-1} $month^{-1}$) and C (dimensionless, ranging between 0 and 1) factors (Eq. 2) (Schmidt et al., 2019):

$$A_{month} = R_{month} \times K \times LS \times C_{month} \times P \quad (2)$$

2.3 Rainfall erosivity factor (R)

The rainfall factor (R), an index unit, reflects the effect of rainfall intensity on soil erosion and requires detailed, continuous precipitation data for its calculation (Wischmeier and Smith, 1978). The R factor is often determined using rainfall intensity and frequency, as they are more predictive compared to the total rainfall amount (Ganasri and Ramesh, 2016; Wynants et al., 2018). However, this information is not readily available for the majority of Sub-Saharan African countries. Moore (1979) observed a strong correlation between the kinetic energy of the high intensity storms in Kenya, Tanzania and Uganda and the mean annual precipitation. Mean monthly rainfall (MMR) data was acquired from The Climate Hazards Group Infrared Precipitation with Stations (CHIRPS) dataset, which is a 30+ year quasi-global rainfall dataset (Funk et al., 2015). Using the regression equation outlined by Moore (1979) and Wynants et al. (2018), the kinetic energy (KE) of the rains (Eq. 3) and the rainfall erosivity factor (R) were calculated (Eq. 4) for each month between January 2017 and June 2020 as shown below:

$$KE = 3.96 \times MMR + 3122 \tag{3}$$

$$R = 17.02(0.029 \times KE - 26) \tag{4}$$

2.4 Soil erodibility factor (K)

The soil erodibility (K) factor was calculated based on intrinsic topsoil (0–20 cm depth) properties (i.e. texture, organic matter, structure, and permeability) from a harmonised dataset derived from the Soil and Terrain Database for Kenya, compiled by the Kenya Soil Survey (Batjes, 2013). Direct measurements of the K factor on field plots are not financially sustainable at regional or national scales. Therefore, the soil erodibility nomograph (Wischmeier et al., 1971) is most commonly used for assessing soil erodibility. An algebraic approximation of the nomograph that includes five soil parameters (texture, organic matter, coarse fragments, structure, and permeability) was proposed by Wischmeier and Smith (1978) and Renard et al. (1997) as shown in Eq. 5:

$$K = [(2.1 \times 10^{-4}\, M^{1.14}(12 - OM) + 3.25(s - 2) + 2.5(p - 3))/100] * 0.1317 \tag{5}$$

Where OM (%) is the organic matter content of the soil, s is the soil structure class (Table S1) and p is the permeability class (Table S2) from Panagos et al. (2014b), respectively and M is the textural factor calculated as shown in Eq. 6

$$M = (msilt + mvfs) \times (100 - mc) \quad (6)$$

In Eq. 6 msilt (%) is the silt fraction content (0.002 – 0.05 mm); mvfs (%) is the very fine sand fraction content (0.05 – 0.1 mm); and mc (%) is the clay fraction content (< 0.002 mm). The very fine sand structure (0.05 – 0.1 mm) as sub-factor (mvfs) in Eq. 6 was estimated as 20% of the sand fraction (0.05 – 2.0 mm) according to Panagos et al. (2014b). The use of these equations has previously been applied in East Africa by Fenta et al. (2020) and Elnashar et al. (2021).

2.5 Topographic factor (LS)

The topographic factor (LS) is the combination of the length (L) and steepness (S) of the slope to determine the impact of topography on soil erosion. As slope length increases, so does the total soil erosion loss per unit due to the progressive accumulation of surface runoff. As the slope steepness increases, so does the velocity and erosivity of runoff (Wischmeier and Smith, 1978). In the present study, the LS factor was computed in ArcGIS based on the digital elevation model (DEM) from the Shuttle Radar Topography Mission (SRTM) with 30 m resolution and derived using ArcGIS (10.3) using Eq. 7 (Mitasova et al., 1996; Pelton et al., 2012; Prasannakumar et al., 2012; Simms et al., 2003).

$$LS = \left(\frac{flow\ acc \times map\ resolution}{22.13}\right)^m \times \left(\frac{\sin slope}{0.09}\right)^n \quad (7)$$

Where flow acc. (accumulation) denotes the accumulated slope effect on a given cell created using Arc hydro tool, map resolution is the dimension of the map grid cell, m and n are slope and area exponent, and sin slope is slope degree of land in sin. The values for m and n, were 0.4 and 1.4, respectively, and were determined based on topographical condition and land use type (Mitasova et al., 1996; Oliveira et al., 2013; Pelton et al., 2012).

2.6 Cover management (C) and conservation support practice factor (P)

The C Factor represents the protective effect of land cover against the erosive action of rainfall. It represents the relationship between soil loss in an area with specific vegetation cover and management and an area with tilled soil, permanently bare during the cropping period, with values closer to 0 corresponding to denser vegetation and values closer to 1 indicate bare land (Durigon et al., 2014; Renard et al., 1997). Due to the variety of land cover patterns with spatial and temporal variations, satellite remote sensing data sets were used for the assessment of the C factor (Prasannakumar et al., 2012). Moderate-Resolution Imaging Spectroradiometer (MODIS) imagery from the Terra platform was used to determine monthly C factors. Normalised Difference Vegetation Index (NDVI) data were obtained at monthly intervals between January 2017 and June 2020 for MODIS tiles 'h21v08' and 'h21v09' from the MODIS-Terra MOD13Q1 product, a 16-day vegetation index composite with a spatial resolution of 250 m. The NDVI, an indicator of the vegetation vigour and health, data was then used to generate the C factor value image for the study area using Eq. 8:

$$C = \left(\frac{-NDVI+1}{2}\right) \quad (8)$$

The P factor accounts for control practices that diminish the erosion potential of runoff by their influence on drainage patterns, runoff concentration, runoff velocity and hydraulic forces exerted by the runoff on the soil surface (Renard et al., 1991). Typically, P factor values close to 0 indicate good conservation practice such as terracing, contour tillage, and permanent barriers or strips reducing the overall risk of erosion, whilst values approaching 1 indicates poor conservation practice. Due to the lack of data regarding conservation practices in the study area, the RUSLE model was run with a P factor of 1.

3. Results and Discussion

3.1 Soil erodibility factor (K)

The K factor values in the Winam Gulf catchment ranged between 0.008 and 0.045 t ha h ha^{-1} MJ^{-1} mm^{-1}, with complex spatial distribution and varying degrees of erodibility within the study area (Figure 2). The highest K factor values (0.045 t ha h ha^{-1} MJ^{-1} mm^{-1}) correspond with mountainous areas, including Nandi Hills in the Nyando sub-basin and the Gwassi Hills in Homa Bay County, located on the Southern Shore of the catchment. The highest degree of K factor heterogeneity occurs in the Kisumu basin at the centre of the catchment; however, the overall risk of soil erodibility in this region remains low due to the topography.

Figure 2 Soil erodibility (K) factor in the Winam Gulf catchment, Kenya

3.2 Topographic factor (LS)

The LS factor values in the study area range from 0 to 38.3, with an average of 2.26 (Figure 3). The study area is dominated by low LS values within the Kisumu basin and land adjacent to the Winam Gulf, as they correspond to flat open plains or wetlands. However, within these areas of low LS values, large river channels have significantly higher LS values due to channel morphology and changes to the riverbank slope (Magesh and Chandrasekar, 2016). Moderately higher LS factors are located to the east of the catchment. The highest LS values are located within the Nandi Hills, Mt Homa, and the Gwassi Hills located on the Southern Shore of the Gulf. All of these areas have steep slopes pertaining to the high LS values.

Figure 3 Topographic (LS) factor in the Winam Gulf catchment, Kenya

3.4 Rainfall erosivity factor (R)

The R factor showed notable spatial variation with clear seasonal and annual changes to the R factor in the Winam Gulf catchment (Figure 4).

Figure 4 Monthly rainfall erosivity (R) factor from January 2017 to June 2020 in the Winam Gulf catchment, Kenya

The R factor value in the study ranges from 92.85 to 180.55 MJ mm ha^{-1} h^{-1} $month^{-1}$. During the rainy season months, the R factor significantly increased compared to dry season months, with the largest R factors typically occurring in April of each year. The trend between the mean R factor (MJ mm ha^{-1} h^{-1} $month^{-1}$) and soil erosion rate (t ha^{-1} $month^{-1}$) in the Winam Gulf over the study period is shown in Figure S1. Previous assessments of intra-annual soil erosion dynamics have shown that the R factor is the most influential aspect of the RUSLE model (Polykretis et al., 2020; Schmidt et al., 2016). However, in this study, no correlation ($r = -0.09$, $p = 0.53$) was associated between the R factor values and the mean monthly soil erosion rate in the Winam Gulf (Figure S2). By using a modified dynamic version of the RUSLE model, Gianinetto et al. (2019) were able to differentiate large seasonal soil erosion variability in the Italian Alps. They conducted sensitivity analysis and indicated that whilst the R factor has the highest impact on the potential soil erosion risk, their pixel-based Pearson's correlation between soil erosion and the R factor was an uncorrelated variable, as replicated in the present study.

3.5 Cover management (C) factor

The C factor analysis performed in this study visualises the dynamic seasonal trends with phases of abundant and fractionated or absent vegetation cover over consecutive years. The dynamic C factor assessment presented here provides key information when determining the presence of soil erosion hot spots, as this process is accelerated on uncovered or bare soil. Low C factor values (<0.15) correspond with areas of vegetation cover and a reduced risk of soil erosion, whereas higher values indicate bare/uncovered land with a greater susceptibility to soil erosion (Figure 5).

Figure 5 Monthly cover management (C) factor from January 2017 to June 2020 in the Winam Gulf catchment, Kenya

During the long rainy season from March to May, vegetation cover increases with a significant reduction ($p < 0.05$) of the mean C factor within the catchment (Table S3). The increased vegetation cover that was initiated by the rains begins to degrade across the catchment throughout the subsequent dry season (from June to September), and as crops were harvested at the end of the growing season. The increased C factor values (reduction in vegetation cover) extend from the Kisumu basin, an area that typically receives the warmest temperatures in the catchment, to the east of the Gulf. Areas to the south and east of the study area (in the Sondu sub-basin) are relatively resilient regions to seasonal changes, as they are dominated by larger forested areas. Following the warmer temperatures from December to February, the highest C factor values occur in January and February, most noticeably in January 2017 and 2018. The extent of this is highly influenced by the variability of the short rainy season in October, leading to an increased risk of erosion. Our results show that soil erosion rates are influenced by seasonal changes to land cover. Gianinetto et al. (2019) reported that the use of multi-temporal satellite data for calculating C factor values highlighted an increased erosion risk in autumn/winter compared to spring/summer in the Italian Alps. The application of dynamic satellite-derived data can increase the spatial resolution of C factor values leading to improved accuracy of the estimates of soil erosion at regional and local scales, particularly where vegetation is the predominant land cover (Gianinetto et al., 2019). The relationship between C factor values and mean soil erosion (t ha^{-1} $month^{-1}$) in the Winam Gulf from January 2017 to June 2020 is shown in Figure S3. There is a strong positive relationship ($r = 0.85$, $p = <0.001$) between the mean C factor and soil erosion in the Winam Gulf (Figure S4). Panagos et al. (2014a) investigated changes to the risk of soil erosion in Crete, Greece using dynamic R and C factors. In their study, the rainy season in Crete (October to January) accounted for 80% of the annual soil erosion on the island. More recently, in the Kyrgyz mountain grasslands, Kulikov et al. (2016) observed that the highest potential soil erosion risk was due to the combined influence of high C factors and simultaneous high R factors. These results stress the importance of seasonal erosion assessments for the identification of erosion hotspots and the sensitivity of RUSLE based models to the status of vegetation cover.

The relationship between the R factor (MJ mm ha^{-1} h^{-1} $month^{-1}$) and the C factor in the Winam Gulf over the study period is shown in Figure S5. The negative trend between the R factor and C factor ($r = -0.60$, $p = <0.001$) (Figure S6) highlights the response of vegetation to increase rainfall. Interestingly, this trend is stronger in the dry season ($r = -0.72$, $p = < 0.001$) compared to the wet season ($r = -0.18$, $p = 0.43$) (Figure S6). Our results support previous assessments of the spatio-temporal correlation between NDVI values and precipitation in the Central Asian region, which indicated time-delayed correlations attributable to vegetation dynamics during growing seasons (Gessner et al., 2013).

3.6 Implications of dynamic soil erosion risk evidence for land management decisions

All RUSLE model factors were integrated using the formula outlined in Eq. (2) and soil erosion maps were created with a spatial resolution of 30 m, representing the loss of soil (t ha^{-1} $month^{-1}$), between January 2017 and June 2020 (Figure 6). The risk of soil erosion ranges from <0.5 to >5 t ha^{-1} $month^{-1}$. Several hotspots were identified within the catchment area; these are typically dominated by steep topography, including the Nandi Hills in the Nyando sub-basin and the Gwassi Hills on the Southern Shore, and have consistently elevated soil erosion risks compared to the relatively flat Kisumu basin, regardless of seasonal changes to R and C factors. Throughout the study, the average soil erosion loss rate for the catchment was 9.63 t ha^{-1} $year^{-1}$, which would hypothetically equate to a total eroded soil mass of 10.71 Mt $year^{-1}$ in the Winam Gulf catchment area. Within the sub-basins, the average soil erosion was 9.69, 12.29, 7.94 and 10.73 t ha^{-1} $year^{-1}$, in the Northern Shore, Nyando, Sondu, and Southern Shore, respectively.

Figure 6 Monthly soil erosion risk from January 2017 to June 2020 in the Winam Gulf catchment, Kenya

Assessing soil erosion with dynamic R and C factors is critical for determining the extent to which changing climatic conditions influence soil erosion, and the potential impact on the socioeconomic stability of subsistence farming communities in Sub-Saharan Africa. The results of this study highlight that the greatest soil erosion rates occur between February and April (0.95 t ha^{-1} $month^{-1}$, Table S3), with additional increased risk in October following drier periods and the short rains. In contrast, between May and August, there is a significantly reduced risk (average soil loss 0.72 t ha^{-1} $month^{-1}$) due to the low rainfall erosivity and increased vegetation cover as a result of the long rainy season. These results demonstrate the lag between rainfall and vegetation growth originally illustrated by Kirkby (1980). These results highlight that the most vulnerable period for erosion is the early part of the wet season when rainfall intensity is increasing with insufficient vegetation growth to protect the soil; as such, peak erosion rates precede peak rainfall. Whilst the validation of soil loss models with *in-situ* plot-scale measurements is desirable it is often constrained by the absence of long-term plot-scale measurements for different land cover types (Fenta et al., 2020). Moreover, plot-scale measurements may be biased due to the highly heterogeneous nature of soil erosion, measurement uncertainty or failure to accurately capture soil loss at the landscape scale (Alewell et al., 2019). Despite these challenges, the modelled RUSLE-based estimated mean soil loss rates in the present study are within the range of soil loss rates reported by other studies based on plot-scale measurements in Kenya (Angima et al., 2000; Kinama et al., 2007). Furthermore, the RULSE model estimated soil erosion rates in this study were validated against previous studies performed in the same region. The results of our study yielded similar predictions to those published by Fenta et al. (2020) who was assessing water and wind erosion risks in the East Africa region. However, additional plot studies are required due to the uncertainty associated with future seasonal weather patterns. Recent climate projections predicted an increasingly vigorous hydrological cycle that could increase global water erosion by +30 to +66%, with some of the most severe impacts affecting Sub-Saharan Africa (Borrelli et al., 2020). Maeda et al. (2010) investigated the potential impacts of climate change on soil erosion in the Kenyan Eastern Arc Mountains and reported that the highest risk of erosion occurred in April and November, associated with higher rainfall during these months. Using a Monte Carlo simulation and synthetic precipitation datasets, Maeda et al. (2010) concluded that there was the possibility of an increased risk of erosion in regions with an elevation greater than 1000 m a.s.l. where precipitation rates are historically higher and experience much higher erosion risk, especially in April and November. Due to the complexity and multifaceted nature of determining soil erosion risk, Maeda et al. (2010) disregarded the impact of dynamic vegetation cover in agricultural areas in their model, which can act as a buffer against the impact of rainfall and soil erosion.

Meusburger et al. (2012) and Schmidt et al. (2016) have previously assessed the effect of combined dynamic R and C factors which can amplify the risk of soil erosion. The overall effectiveness of a crop reducing erosion risk depends largely on how much of the erosive rain occurs during those periods when the crop is absent and provides little to no protection (Wischmeier and Smith, 1965).

Months with, and following, the highest rainfall usually coincide with periods of maximum vegetation vigour, and the months of lower rainfall with the seeding and harvest. In the present study, evidence of this is demonstrated in May, which on average receives some of the highest rainfall and associated R factors, yet the risk of erosion is significantly decreased due to lower C factors. The decreased C factor is resulting from the high rainfall in April, which promotes greater crop growth and vegetation cover, thus limiting the erosion risk. In contrast, January and February, which on average have the lowest R factors, have erosion risks that are attributable to the high C factor and lack of vegetation.

There are numerous benefits of assessing soil loss rates with monthly temporal resolution compared to annual rates. Comparing the pseudo average monthly soil loss rate of 0.80 t ha^{-1} (Table S3) against the calculated monthly loss rates would lead to an underestimation of soil loss in dry seasons and an overestimation during the rainy seasons. The higher temporal resolution achieved by monthly modelling provides greater knowledge regarding particularly vulnerable months (January to April), and can inform future strategies for targeted mitigation measures. In a recent study quantifying soil losses in Kenya coastal region, Hategekimana et al. (2020) suggested that areas with an annual average soil erosion >10 t ha^{-1} $year^{-1}$ should be prioritised in soil conservation plans. Based on their recommendations, a significant area of the Winam Gulf would require prioritising, particularly in the Nyando and Southern Shore sub-basins.

3.7 Limitations, uncertainties and needs

The primary limitation to this study was the omission of the analysis of the management practice (P) factor. Gianinetto et al. (2019) and Maeda et al. (2010) have previously stated that the assessment of soil erosion risk could be further refined by introducing a parametrisation for the P factor. The application and maintenance of support practise measures can substantially decrease the risk of soil erosion. Conservation practices such as contour farming, strip cropping, or terracing can reduce RUSLE estimated soil loss by a factor of 2, 4, and 10, respectively (Schürz et al., 2020). In practice, Terranova et al. (2009) in Calabria, Italy, and Feng et al. (2010) in the Loess Plateau, China, have demonstrated that soil conservation measures can significantly decrease the risk of soil erosion. Hence, further investigation is required to evaluate the potential of using conservation farming practices that mitigate the impact of soil erosion in the Winam Gulf, with particular emphasis on reducing the risk of erosion in the region. It is important to acknowledge the uncertainty contribution in the soil erosion calculations derived from using precipitation, DEM, soil, and NDVI data with different spatial resolutions. Soil erosion modelling is inherently influenced by the accuracy of these variables, and input data with finer spatial resolutions yield more accurate risk assessments (Guo et al., 2021). Whilst the RUSLE model has its limitations, it is widely used due to its relative simplicity and robustness. This approach is capable of facilitating soil conservation policies at national and multinational scales as local methodologies may suffer from poor consistency and high levels of uncertainty (Panagos et al., 2016; Rellini et al., 2019). Notwithstanding the limitations, the information provided in this study has identified areas in the Winam Gulf catchment, primarily within the Nandi Hills and Gwassi Hills, which require further investigation to assess the full extent of soil erosion. Field-based studies capable of incorporating existing conservation practices are recommended in areas prone to significant soil erosion risk to determine actual soil loss rates. This will aid decision-making enabling stakeholders and policymakers to target specific management efforts for reducing soil erosion.

4. Conclusion

The soil erosion maps presented here provide the first assessment of erosion risk with monthly temporal resolution in Sub-Saharan Africa, considering dynamic rainfall and vegetation cover datasets. They enable the quantification of soil erosion and provide information regarding spatio-temporal patterns of soil loss due to water erosion in the Winam Gulf. Our RUSLE model outputs showed that the mean annual gross soil loss by water erosion is approximately 10.71 Mt year^{-1} with a mean soil loss rate of 9.63 t ha^{-1} year^{-1}. These results show that the highest risk occurs between January and April, which coincides with periods of reduced vegetation cover and high rainfall. We demonstrated the need to assess soil erosion with greater temporal resolution than annual assessments, due to seasonal variability leading to the under and overestimation of soil erosion by water in specific months. Moreover, as the effects of climate change on precipitation patterns are projected to increase the risk of soil erosion a greater level of understanding is essential to evaluate how to best implement soil conservation practices.

Acknowledgements

Funding for this research was provided by The Royal Society (grant number: ICA\R1\1910770 and NERC-UKRI ODA-NC Foundation Award. The authors would like to thank Dr Maarten Wynants and Dr Elliott Hamilton for their contributions to the paper. In addition, the authors would like to thank all data providers for making their data available. This work is published with the permission of the Executive Director, British Geological Survey.

References

Alewell C, Borrelli P, Meusburger K, Panagos P. Using the USLE: Chances, challenges and limitations of soil erosion modelling. International Soil and Water Conservation Research 2019; 7: 203-225.

Alexandridis TK, Sotiropoulou AM, Bilas G, Karapetsas N, Silleos NG. The effects of seasonality in estimating the C-factor of soil erosion studies. Land Degradation & Development 2015; 26: 596-603.

Amundson R, Berhe AA, Hopmans JW, Olson C, Sztein AE, Sparks DL. Soil and human security in the 21st century. Science 2015; 348.

Angima S, O'Neill M, Omwega A, Stott D. Use of tree/grass hedges for soil erosion control in the Central Kenyan highlands. Journal of soil and water conservation 2000; 55: 478-482.

Angulo-Martínez M, Beguería S. Estimating rainfall erosivity from daily precipitation records: A comparison among methods using data from the Ebro Basin (NE Spain). Journal of Hydrology 2009; 379: 111-121.

Bakker MM, Govers G, Jones RA, Rounsevell MD. The effect of soil erosion on Europe's crop yields. Ecosystems 2007; 10: 1209-1219.

Ballabio C, Borrelli P, Spinoni J, Meusburger K, Michaelides S, Beguería S, et al. Mapping monthly rainfall erosivity in Europe. Science of the Total Environment 2017; 579: 1298-1315.

Batjes NH. SOTER-based soil parameter estimates (SOTWIS) for Kenya (version 1.0), 2013.

Blaikie P, Brookfield H. Land degradation and society: Routledge, 2015.

Borrelli P, Robinson DA, Fleischer LR, Lugato E, Ballabio C, Alewell C, et al. An assessment of the global impact of 21st century land use change on soil erosion. Nature Communications 2017; 8: 2013.

Borrelli P, Robinson DA, Panagos P, Lugato E, Yang JE, Alewell C, et al. Land use and climate change impacts on global soil erosion by water (2015-2070). Proceedings of the National Academy of Sciences 2020; 117: 21994-22001.

Brink AB, Eva HD. Monitoring 25 years of land cover change dynamics in Africa: A sample based remote sensing approach. Applied geography 2009; 29: 501-512.

Calamari D, Akech M, Ochumba P. Pollution of Winam Gulf, Lake Victoria, Kenya: A case study for preliminary risk assessment. Lakes & Reservoirs: Research & Management 1995; 1: 89-106.

Chen T, Niu R-q, Li P-x, Zhang L-p, Du B. Regional soil erosion risk mapping using RUSLE, GIS, and remote sensing: a case study in Miyun Watershed, North China. Environmental Earth Sciences 2011; 63: 533-541.

Durigon VL, Carvalho DF, Antunes MAH, Oliveira PTS, Fernandes MM. NDVI time series for monitoring RUSLE cover management factor in a tropical watershed. International Journal of Remote Sensing 2014; 35: 441-453.

Elnashar A, Zeng H, Wu B, Fenta AA, Nabil M, Duerler R. Soil erosion assessment in the Blue Nile Basin driven by a novel RUSLE-GEE framework. Science of The Total Environment 2021; 793: 148466.

Feng X, Wang Y, Chen L, Fu B, Bai G. Modeling soil erosion and its response to land-use change in hilly catchments of the Chinese Loess Plateau. Geomorphology 2010; 118: 239-248.

Fenta AA, Tsunekawa A, Haregeweyn N, Poesen J, Tsubo M, Borrelli P, et al. Land susceptibility to water and wind erosion risks in the East Africa region. Science of The Total Environment 2020; 703: 135016.

Funk C, Peterson P, Landsfeld M, Pedreros D, Verdin J, Shukla S, et al. The climate hazards infrared precipitation with stations—a new environmental record for monitoring extremes. Scientific Data 2015; 2: 150066.

Fusilli L, Collins M, Laneve G, Palombo A, Pignatti S, Santini F. Assessment of the abnormal growth of floating macrophytes in Winam Gulf (Kenya) by using MODIS imagery time series. International journal of applied earth observation and geoinformation 2013; 20: 33-41.

Ganasri BP, Ramesh H. Assessment of soil erosion by RUSLE model using remote sensing and GIS - A case study of Nethravathi Basin. Geoscience Frontiers 2016; 7: 953-961.

Gessner U, Naeimi V, Klein I, Kuenzer C, Klein D, Dech S. The relationship between precipitation anomalies and satellite-derived vegetation activity in Central Asia. Global and Planetary Change 2013; 110: 74-87.

Gianinetto M, Aiello M, Polinelli F, Frassy F, Rulli MC, Ravazzani G, et al. D-RUSLE: A dynamic model to estimate potential soil erosion with satellite time series in the Italian Alps. European Journal of Remote Sensing 2019; 52: 34-53.

Guo L, Liu R, Men C, Wang Q, Miao Y, Shoaib M, et al. Multiscale spatiotemporal characteristics of landscape patterns, hotspots, and influencing factors for soil erosion. Science of The Total Environment 2021; 779: 146474.

Hategekimana Y, Allam M, Meng Q, Nie Y, Mohamed E. Quantification of Soil Losses along the Coastal Protected Areas in Kenya. Land 2020; 9: 137.

Igwe P, Onuigbo A, Chinedu O, Ezeaku I, Muoneke M. Soil erosion: a review of models and applications. International Journal of Advanced Engineering Research and Science 2017; 4: 237341.

Istvánovics V. Eutrophication of lakes and reservoirs. Lake ecosystem ecology. Elsevier, San Diego, CA 2010: 47-55.

IUSS Working Group W. World reference base for soil resources 2014. International soil classification system for naming soils and creating legends for soil maps. World Soil Resources Report 2014; 106.

Kinama J, Stigter C, Ong C, Ng'ang'a J, Gichuki F. Contour hedgerows and grass strips in erosion and runoff control on sloping land in semi-arid Kenya. Arid land research and management 2007; 21: 1-19.

Kirkby M. the problem'in Kirkby, MJ and Morgan, RPC (eds) Soil Erosion. Chichester, Wiley 1980; 1: 16.

Kouli M, Soupios P, Vallianatos F. Soil erosion prediction using the revised universal soil loss equation (RUSLE) in a GIS framework, Chania, Northwestern Crete, Greece. Environmental Geology 2009; 57: 483-497.

Kulikov M, Schickhoff U, Borchardt P. Spatial and seasonal dynamics of soil loss ratio in mountain rangelands of south-western Kyrgyzstan. Journal of Mountain Science 2016; 13: 316-329.

Lu D, Li G, Valladares GS, Batistella M. Mapping soil erosion risk in Rondônia, Brazilian Amazonia: using RUSLE, remote sensing and GIS. Land Degradation & Development 2004; 15: 499-512.

Ma X, He Y, Xu J, van Noordwijk M, Lu X. Spatial and temporal variation in rainfall erosivity in a Himalayan watershed. Catena 2014; 121: 248-259.

Maeda EE, Pellikka PK, Siljander M, Clark BJ. Potential impacts of agricultural expansion and climate change on soil erosion in the Eastern Arc Mountains of Kenya. Geomorphology 2010; 123: 279-289.

Magesh N, Chandrasekar N. Assessment of soil erosion and sediment yield in the Tamiraparani sub-basin, South India, using an automated RUSLE-SY model. Environmental Earth Sciences 2016; 75: 1208.

Meusburger K, Steel A, Panagos P, Montanarella L, Alewell C. Spatial and temporal variability of rainfall erosivity factor for Switzerland. Hydrol. Earth Syst. Sci. 2012; 16: 167-177.

Mitasova H, Hofierka J, Zlocha M, Iverson LR. Modelling topographic potential for erosion and deposition using GIS. International Journal of Geographical Information Systems 1996; 10: 629-641.

Moore T. Rainfall erosivity in east Africa. Geografiska Annaler: Series A, Physical Geography 1979; 61: 147-156.

Nearing MA, Jetten V, Baffaut C, Cerdan O, Couturier A, Hernandez M, et al. Modeling response of soil erosion and runoff to changes in precipitation and cover. CATENA 2005; 61: 131-154.
Nunes AN, Lourenço L, Vieira A, Bento-Gonçalves A. Precipitation and erosivity in southern Portugal: seasonal variability and trends (1950–2008). Land Degradation & Development 2016; 27: 211-222.
Obalum SE, Buri MM, Nwite JC, Watanabe Y, Igwe CA, Wakatsuki T. Soil degradation-induced decline in productivity of Sub-Saharan African soils: The prospects of looking downwards the lowlands with the sawah ecotechnology. Applied and Environmental Soil Science 2012; 2012.
Okungu J, Njoka S, Abuodha J, Hecky R. An introduction to Lake Victoria catchment, water quality, physical limnology and ecosystem status (Kenyan sector). Lake Victoria environment report water quality and ecosystem status: Kenya national water quality synthesis report. Lake Victoria Environment Management Project (LVEMP), Kisumu 2005: 1-27.
Oldeman LR. Global extent of soil degradation. Bi-Annual Report 1991-1992/ISRIC. ISRIC, 1992, pp. 19-36.
Oliveira PTS, Rodrigues DBB, Sobrinho TA, Panachuki E, Wendland E. Use of SRTM data to calculate the (R) USLE topographic factor. Acta Scientiarum. Technology 2013; 35: 507-513.
Panagos P, Borrelli P, Poesen J, Meusburger K, Ballabio C, Lugato E, et al. Reply to "The new assessment of soil loss by water erosion in Europe. Panagos P. et al., 2015 Environ. Sci. Policy 54, 438–447—A response" by Evans and Boardman [Environ. Sci. Policy 58, 11–15]. Environmental Science & Policy 2016; 59: 53-57.
Panagos P, Christos K, Cristiano B, Ioannis G. Seasonal monitoring of soil erosion at regional scale: An application of the G2 model in Crete focusing on agricultural land uses. International Journal of Applied Earth Observation and Geoinformation 2014a; 27: 147-155.
Panagos P, Karydas CG, Gitas IZ, Montanarella L. Monthly soil erosion monitoring based on remotely sensed biophysical parameters: a case study in Strymonas river basin towards a functional pan-European service. International Journal of Digital Earth 2012; 5: 461-487.
Panagos P, Meusburger K, Ballabio C, Borrelli P, Alewell C. Soil erodibility in Europe: A high-resolution dataset based on LUCAS. Science of The Total Environment 2014b; 479-480: 189-200.
Pelton J, Frazier E, Pickilingis E. Calculating slope length factor (LS) in the revised Universal Soil Loss Equation (RUSLE), 2012.
Pimentel D. Soil erosion: a food and environmental threat. Environment, development and sustainability 2006; 8: 119-137.
Polykretis C, Alexakis DD, Grillakis MG, Manoudakis S. Assessment of intra-annual and inter-annual variabilities of soil erosion in Crete Island (Greece) by incorporating the Dynamic "Nature" of R and C-Factors in RUSLE modeling. Remote Sensing 2020; 12: 2439.
Prasannakumar V, Vijith H, Abinod S, Geetha N. Estimation of soil erosion risk within a small mountainous sub-watershed in Kerala, India, using Revised Universal Soil Loss Equation (RUSLE) and geo-information technology. Geoscience Frontiers 2012; 3: 209-215.
Rellini I, Scopesi C, Olivari S, Firpo M, Maerker M. Assessment of soil erosion risk in a typical Mediterranean environment using a high resolution RUSLE approach (Portofino promontory, NW-Italy). Journal of Maps 2019; 15: 356-362.
Renard KG, Foster GR, Weesies G, McCool D, Yoder D. Predicting soil erosion by water: a guide to conservation planning with the Revised Universal Soil Loss Equation (RUSLE). Vol 703: United States Department of Agriculture Washington, DC, 1997.
Renard KG, Foster GR, Weesies GA, Porter JP. RUSLE: Revised universal soil loss equation. Journal of soil and Water Conservation 1991; 46: 30-33.
Schmidt S, Alewell C, Meusburger K. Mapping spatio-temporal dynamics of the cover and management factor (C-factor) for grasslands in Switzerland. Remote Sensing of Environment 2018; 211: 89-104.
Schmidt S, Alewell C, Meusburger K. Monthly RUSLE soil erosion risk of Swiss grasslands. Journal of Maps 2019; 15: 247-256.
Schmidt S, Alewell C, Panagos P, Meusburger K. Regionalization of monthly rainfall erosivity patterns in Switzerland. Hydrology and Earth System Sciences 2016; 20: 4359-4373.
Schürz C, Mehdi B, Kiesel J, Schulz K, Herrnegger M. A systematic assessment of uncertainties in large-scale soil loss estimation from different representations of USLE input factors – a case study for Kenya and Uganda. Hydrol. Earth Syst. Sci. 2020; 24: 4463-4489.
Simms A, Woodroffe C, Jones B. Application of RUSLE for erosion management in a coastal catchment, southern NSW. 2003.
Terranova O, Antronico L, Coscarelli R, Iaquinta P. Soil erosion risk scenarios in the Mediterranean environment using RUSLE and GIS: an application model for Calabria (southern Italy). Geomorphology 2009; 112: 228-245.
Troxler J, Chatelain C, Schwery M. Technical and economical evaluation of grazing systems for high altitude sheep pastures in Switzerland. Land use systems in grassland dominated regions. Proceedings of the

20th General Meeting of the European Grassland Federation, Luzern, Switzerland, 21-24 June 2004. vdf Hochschulverlag AG an der ETH Zurich, 2004, pp. 590-592.

Van Oost K, Govers G, Desmet P. Evaluating the effects of changes in landscape structure on soil erosion by water and tillage. Landscape ecology 2000; 15: 577-589.

Vrieling A. Satellite remote sensing for water erosion assessment: A review. Catena 2006; 65: 2-18.

Wang G, Gertner G, Liu X, Anderson A. Uncertainty assessment of soil erodibility factor for revised universal soil loss equation. Catena 2001; 46: 1-14.

Wischmeier W, Smith D. Predicting Rainfall-Erosion-Losses from Cropland East of the Rocky Mountains: A Guide for Selection of Practices for Soil and Water Conservation. US Department of Agricultural, Washington DC, USA 1965.

Wischmeier WH, Johnson C, Cross B. Soil erodibility nomograph for farmland and construction sites. Journal of soil and water conservation 1971.

Wischmeier WH, Smith DD. Predicting rainfall erosion losses-a guide to conservation planning. Predicting rainfall erosion losses-a guide to conservation planning. 1978.

Wynants M, Kelly C, Mtei K, Munishi L, Patrick A, Rabinovich A, et al. Drivers of increased soil erosion in East Africa’s agro-pastoral systems: changing interactions between the social, economic and natural domains. Regional Environmental Change 2019; 19: 1909-1921.

Wynants M, Solomon H, Ndakidemi P, Blake WH. Pinpointing areas of increased soil erosion risk following land cover change in the Lake Manyara catchment, Tanzania. International Journal of Applied Earth Observation and Geoinformation 2018; 71: 1-8.

Yang D, Kanae S, Oki T, Koike T, Musiake K. Global potential soil erosion with reference to land use and climate changes. Hydrological processes 2003; 17: 2913-2928.

Yang X. Deriving RUSLE cover factor from time-series fractional vegetation cover for hillslope erosion modelling in New South Wales. Soil Research 2014; 52: 253-261.

Zuazo VcHD, Pleguezuelo CRoR. Soil-erosion and runoff prevention by plant covers: a review. Sustainable agriculture. Springer, 2009, pp. 785-811.

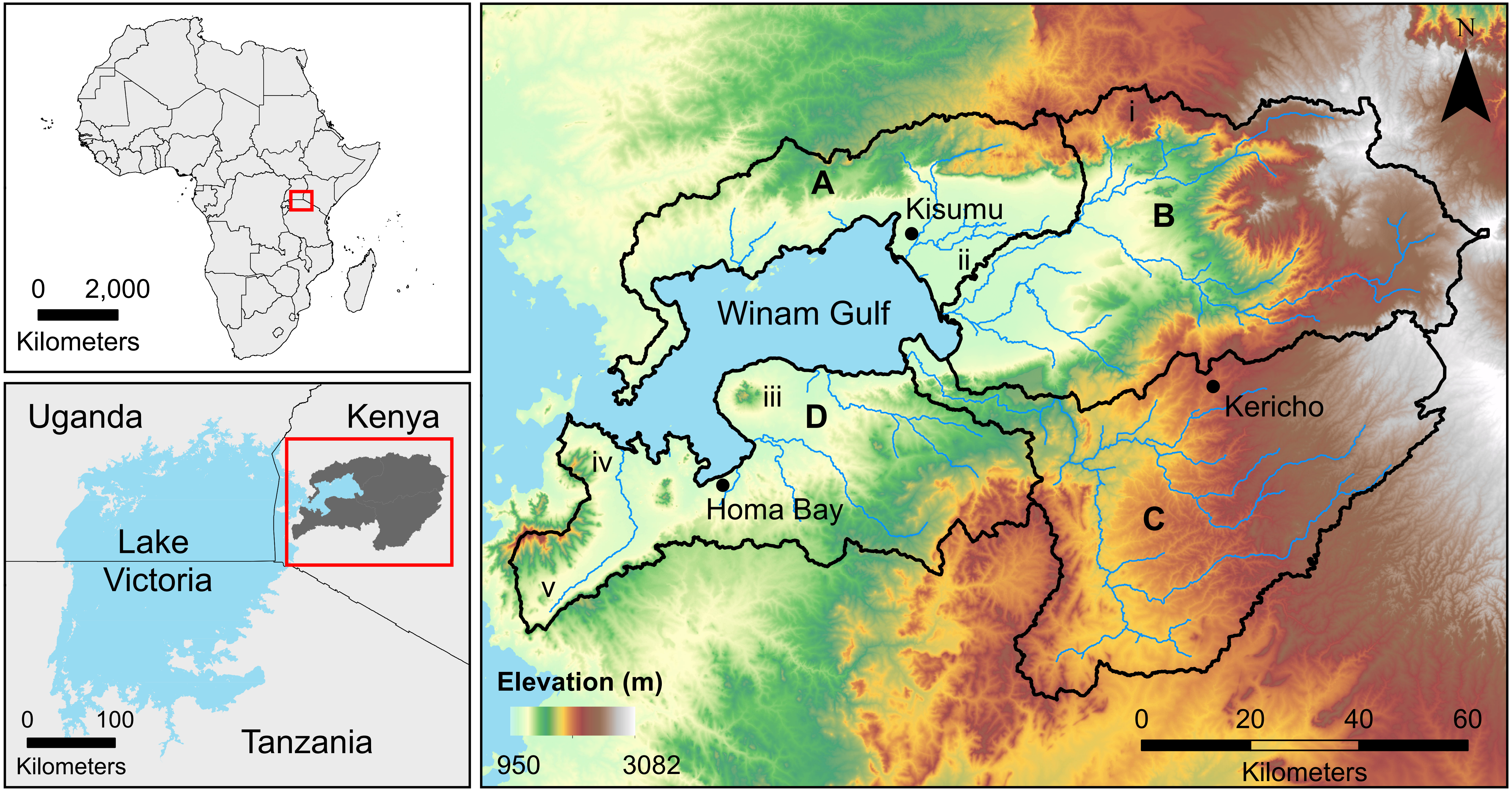
0
2,000
Kilometers
Uganda
Kenya
Lake
Victoria
0
100
Kilometers
Tanzania
N
A
B
C
D
i
ii
iii
iv
v
Kisumu
Winam Gulf
Kericho
Homa Bay
Elevation (m)
950
3082
0
20
40
60
Kilometers

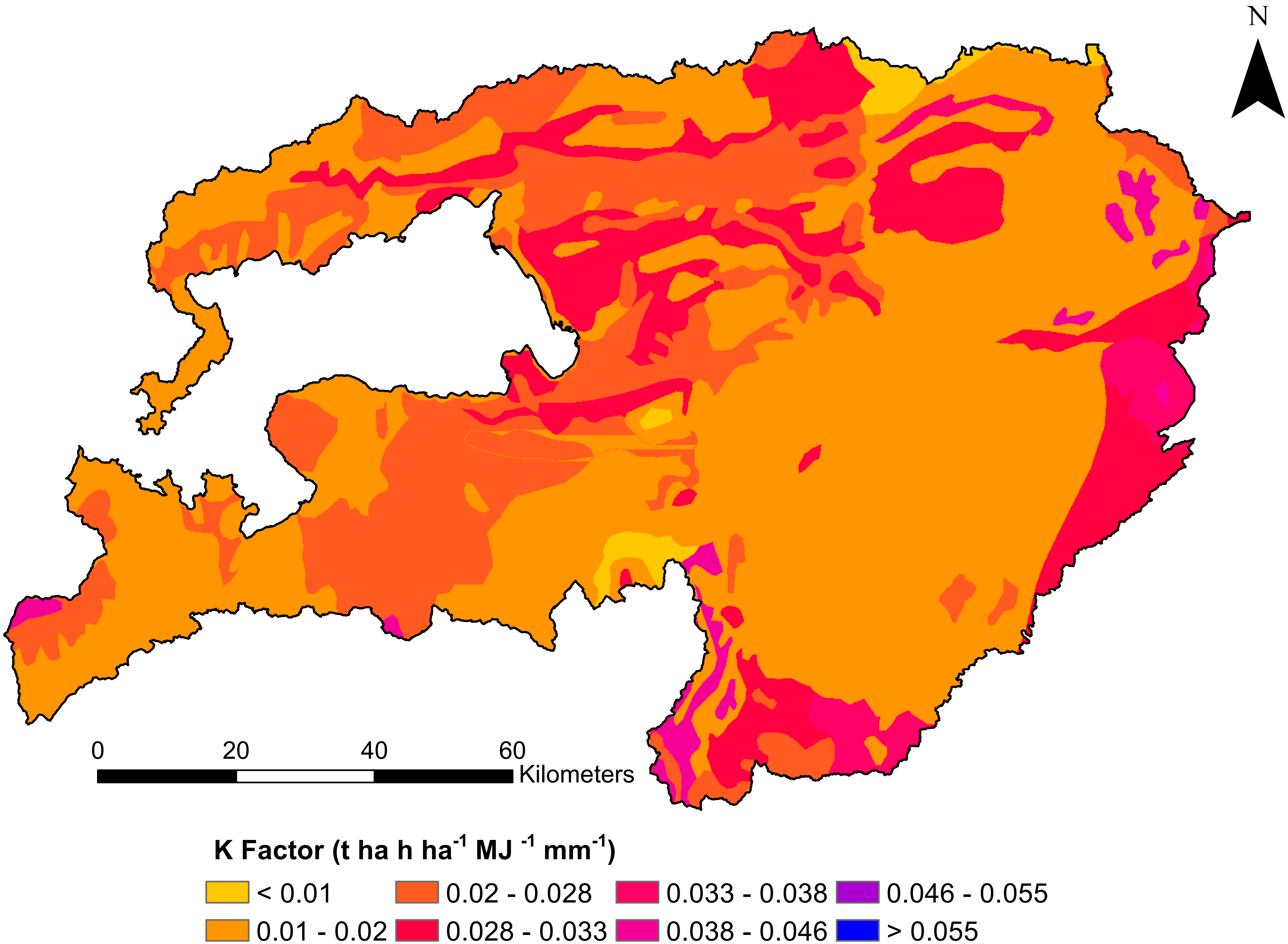
N
0
20
40
60
Kilometers
K Factor (t ha h ha-1 MJ -1 mm-1)
< 0.01
0.01 - 0.02
0.02 - 0.028
0.028 - 0.033
0.033 - 0.038
0.038 - 0.046
0.046 - 0.055
> 0.055

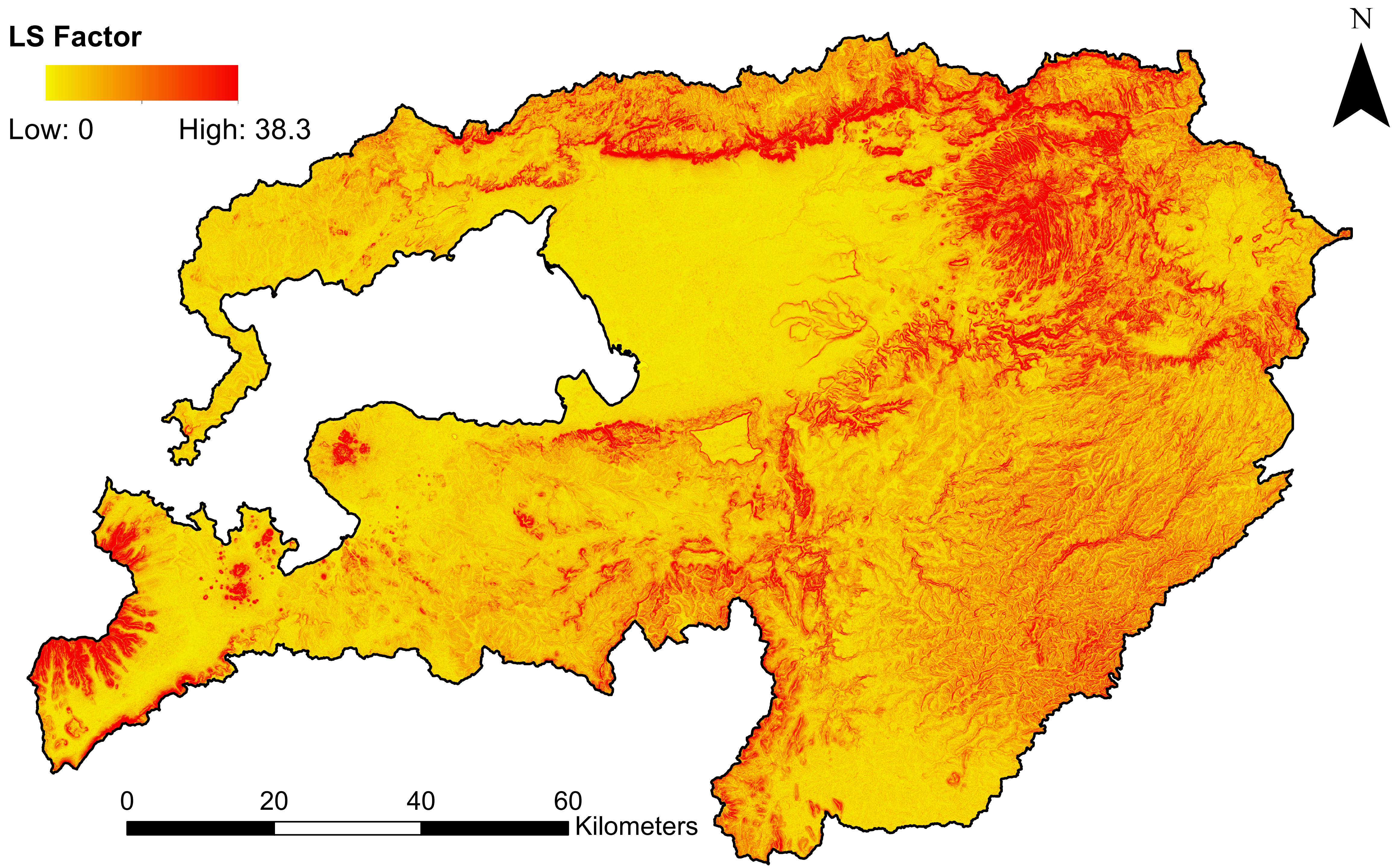
LS Factor
Low: 0
High: 38.3
N
0
20
40
60
Kilometers


Jan 2017
Feb 2017
Mar 2017
Apr 2017
May 2017
Jun 2017
Jul 2017
Aug 2017
Sept 2017
Oct 2017
Nov 2017
Dec 2017
Jan 2018
Feb 2018
Mar 2018
Apr 2018
May 2018
Jun 2018
Jul 2018
Aug 2018
Sept 2018
Oct 2018
Nov 2018
Dec 2018
Jan 2019
Feb 2019
Mar 2019
Apr 2019
May 2019
Jun 2019
Jul 2019
Aug 2019
Sept 2019
Oct 2019
Nov 2019
Dec 2019
Jan 2020
Feb 2020
Mar 2020
Apr 2020
May 2020
Jun 2020
R Factor (MJ mm ha-1 h-1 month-1)
Low : 92.85
High : 180.55


Jan 2017
Feb 2017
Mar 2017
Apr 2017
May 2017
Jun 2017
Jul 2017
Aug 2017
Sept 2017
Oct 2017
Nov 2017
Dec 2017
Jan 2018
Feb 2018
Mar 2018
Apr 2018
May 2018
Jun 2018
Jul 2018
Aug 2018
Sept 2018
Oct 2018
Nov 2018
Dec 2018
Jan 2019
Feb 2019
Mar 2019
Apr 2019
May 2019
Jun 2019
Jul 2019
Aug 2019
Sept 2019
Oct 2019
Nov 2019
Dec 2019
Jan 2020
Feb 2020
Mar 2020
Apr 2020
May 2020
Jun 2020
C Factor
< 0.1
0.1 - 0.15
0.15 - 0.2
0.2 - 0.25
0.25 - 0.3
0.3 - 0.35
0.35 - 0.4
> 0.4

Jan 2017
Feb 2017
Mar 2017
Apr 2017
May 2017
Jun 2017
Jul 2017
Aug 2017
Sept 2017
Oct 2017
Nov 2017
Dec 2017
Jan 2018
Feb 2018
Mar 2018
Apr 2018
May 2018
Jun 2018
Jul 2018
Aug 2018
Sept 2018
Oct 2018
Nov 2018
Dec 2018
Jan 2019
Feb 2019
Mar 2019
Apr 2019
May 2019
Jun 2019
Jul 2019
Aug 2019
Sept 2019
Oct 2019
Nov 2019
Dec 2019
Jan 2020
Feb 2020
Mar 2020
Apr 2020
May 2020
Jun 2020
Soil Erosion (t ha^{-1} month^{-1})
< 0.1
0.1 - 0.5
0.5 - 0.75
0.75 - 1
1 - 1.5
1.5 - 2.5
2.5 - 5
> 5